Silica optical fibre drawn from 3D printed preforms

YUSHI CHU,[1,2,4] XINGHU FU,[2,3] YANHUA LUO,[2] JOHN CANNING,[1,*] YUAN TIAN,[2] KEVIN COOK,[1] JIANZHONG ZHANG,[4] AND GANG-DING PENG[2]

[1]*interdisciplinary Photonics Laboratories, Tech Lab, School of Electrical & Data Engineering, University of Technology Sydney, NSW 2007 & 2019 Australia*

[2]*Photonics and Optical Communications, School of Electrical Engineering and Telecommunications, University of New South Wales, Sydney, NSW 2052, Australia*

[3]*Key Laboratory for Special Fiber and Fiber Sensor of Hebei Province, School of Information Science and Engineering, Yanshan University, Qinhuangdao, 066004, China*

[4]*Key Laboratory of In-fiber Integrated Optics of Ministry of Education, School of Science, Harbin Engineering University, Harbin 150001, China*

**Corresponding author: John.Canning@uts.edu.au*

Received XX Month XXXX; revised XX Month, XXXX; accepted XX Month XXXX; posted XX Month XXXX (Doc. ID XXXXX); published XX Month XXXX

Silica optical fibre was drawn from a three-dimensional (3D) printed preform. Both single mode and multimode fibres are reported. The results demonstrate additive manufacturing of glass optical fibres and its potential to disrupt traditional optical fibre fabrication. It opens up fibre designs for novel applications hitherto not possible.

http://dx.doi.org/10.1364/OL.99.099999

Silica optical fibres are the backbone of both the global telecommunications and internet-of things (IoT) networks [1-2]. Other fibre materials fill niche gaps, such as low-cost multimode polymer fibres for data networks. These have recently experienced a major fabrication disruption arising from the proposal and subsequent introduction of optical preforms fabricated using additive manufacturing methods [3-4]. Such methods use bottom-up 3D printing that can circumvent traditional assembly with lathe-based or manual stack-and-draw approaches [5-10]. These conventional methods often share the significant limitation of being centre-derived assembly methods, shaped by a central axis in a spinning lathe. Additive manufacture, or 3D printing, by contrast promises to disrupt this space. Further, beyond preform fabrication, the idea of entirely drawing fibre from a 3D printer has been proposed and demonstrated [11], capitalized upon by others [12]. However, despite these and other innovations that followed, silica remains the holy grail of 3D printing optical fibre because of is ubiquity and low loss against which no niche alternative can compete. This is a grand challenge that needs to be met. Here, we report the first demonstration of additive manufacturing of a silica based preform using both 3D printing and thermal processing.

One of the challenges with 3D printing silica fibres is the ultra-high temperatures required, often exceeding T = 1900 °C. The practical issue of developing technology that can handle such temperatures when melting the glass and moving it around on an *xyz* stage has impeded development in this area. Nonetheless, glass printing has been reported, including a brute force approach using fused deposition modelling (FDM) with high temperature zirconate nozzles to pump through molten silica [13]. Unfortunately, this approach was also stymied by the high viscosity of the glass, limiting practical printing at this stage to a resolution of ~ 4 mm, ten times worse than common plastic based FDM. To circumvent the extraordinarily high temperatures required, hybrid or composite material using a lower melting polymer with either organic encapsulated silica [14-15] or nano or micro particles of glass has been reported [16]. The first 3D printed transparent fused silica glass extending several millimeters but with micron resolution, was achieved using ultraviolet (UV) sensitive monomer suspended with silica and direct light project (DLP) 3D printing or direct laser writing [17-18]. Similar methods were used based on direct ink writing (DIW) to obtain several centimeter long samples with sub-millimeter resolution [19-20]. These latter methods used sol-gel silica suspended in an aqueous organic solution. Overall the main processes are similar involving material formulation to reduce thermal temperatures, photo- or thermal-polymerization to solidify the liquid state and subsequent polymer annealing. This was followed by debinding and removal of the polymer and impurities before fusing the silica through sintering at higher temperatures.

Here, in this letter, we extend the work on hybrid polymer-glass mix and DLP printing. By controlling the silica nanoparticle size and homogeneity, we can produce glass samples with dimensions exceeding 10 cm, necessary for optical preform work.

A summary of the printing method used for step-index optical fibres is shown in Figure 1. The steps involve photocurable resin preparation, 3D printing of preforms, core fabrication, thermal debinding and final fibre drawing. Amorphous silica nanoparticles (ϕ ~ 40 nm, Aerosil OX50, Supplier: Evonik, Australia) were dispersed in photocurable resin, shown in Fig. 1(a). The photocurable resin was fabricated by mixing 2-hydroxyethyl

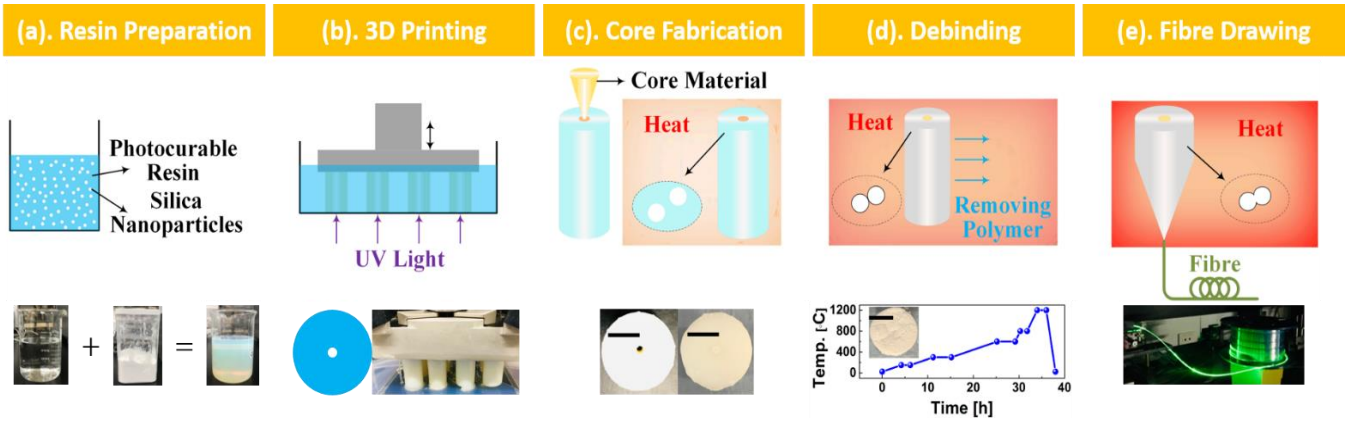

Fig. 1. Fabrication of the step-index silica optical fibre using 3D printing: (a) dispersion of silica nanoparticle into ultraviolet curable resin; (b) DLP 3D printing with UV light at 385 nm; (c) core material was poured into printed preform and undertaken a further thermal curing; (d) debinding process to remove organic binder; and finally (e) fibre drawing. All scale bars shown are 10 mm.

methacrylate (HEMA), 2-phenoxyethanol (POE), tetra(ethylenglycol) diacrylate (TEGDA), diphenyl(2,4,6-trimethylbenzoyl) phosphine oxide (DPO) and hydroquinone (Hyd), all of which were purchased from Sigma-Aldrich, Australia. The composition of the combined printing resin was 37.4 wt% SiO_2, 36.9 wt % HEMA, 19.0 wt % POE, 6.36 wt% TEGDA, 0.2 wt% DPO, and 0.1 wt% Hyd. This mixed resin was polymerized with the DLP 3D printer using λ = 385 nm (Asiga Freeform Pro 2 75 UV; *x,y* pixel resolution ~ 75 μm). By avoiding traditional optical fibre preform fabrication using a centre-spun lathe, it is possible to produce arbitrary structures. However, the aim of this Letter is to demonstrate the first 3D printed silica optical fibres, choosing to focus on the step-index silica fibre as proof of concept and as reference.

The preform structure was designed on Inventor CAD (inner/outer diameter ratio, $\phi_{inner}/\phi_{outer}$ = 3/25 mm and length, L = 20 - 100 mm). The preform was printed layer-by-layer using UV light traversed in the vertical direction - see Fig. 1(b) (I_{UV} = 5.8 mW/cm^2, t_{curing} = 3.5 s, layer thickness τ = 75 μm).

The step-index core was fabricated by inserting a prepared resin into the centre hole of the printed cladding preform, illustrated in Fig. 1(c). GeO_2, TiO_2 and 2,2-azobis(2-methylpropionitrile) or AIBN (all from Sigma-Aldrich) were added to increase the refractive index. The final core resin composition contained 32.6 wt% SiO_2, 38.6 wt% HEMA, 19.9 wt% POE, 6.65 wt% TEGDA, 0.2 wt% DPO, 0.1 wt% Hyd, 0.5 wt% AIBN, 1.2 wt% GeO_2, and 0.84 wt% TiO_2. The core resin was poured into the cladding hole and cured at T = 60 °C for t = 2 hrs and T = 90 °C for t = 0.5hrs, similar to [21-22].

The fabricated preform was subsequently subjected to thermal debinding, where the polymer and other impurities are removed, illustrated in Fig. 1(d). During debinding, the organic components were removed. Five temperature stages were employed: 150, 300, 600, 800 and 1200 °C for 2, 4, 4, 1.5 and 2 h respectively, with heating rate dT/dt = 0.5 °C/min up to T = 600 °C and dT/dt = 3 °C/min after 600 °C. The corresponding shrinkage and weight loss with polymer removal leaves behind an inorganic solid glass held together primarily by van der Waals force and perhaps some partial sintering. The size of preforms reduced predictably after debinding, consistent with their concentrations: the outer diameter, inner diameter and height decreased 30%, 34% and 23% respectively. These are important parameters for integrating this shrinkage into the fibre design of single and multicore fibres generally.

After debinding, the preform was inserted into a Heraeus F300 quartz tube for support and drawn directly into fibre on a commercial drawing tower (Fig. 1(e)). The drawing temperature (T ~ 1855 °C) was slightly lower than normal MCVD processing to help remove air, water and residual polymer gradually. The inner pressure of the preform was kept as low as possible (P ~ 50 mbar). Finally, fibres of length L ~ 2.3 km were readily drawn, shown in Figure 1(e). During this process, the changes in the silica nanoparticles is illustrated by the dashed ellipses shown in Fig. 1(c), (d) and (e). Those enlarged white dots represented silica nanoparticles whilst the blue background represents the polymer binder. As the temperature gradually increased, the polymer is ablated leaving behind the silica nanoparticles, which come closer together leading to preform shrinkage. Sintering at higher temperatures fuses them together.

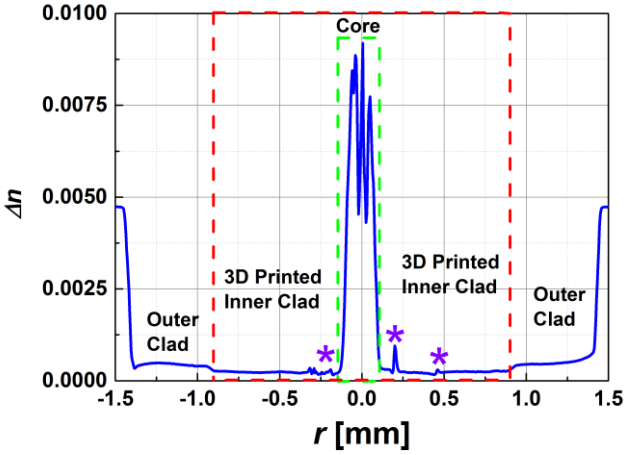

Fig. 2. Refractive index difference profile (Δn vs r) of the 3D printed and sintered preform. The stars identify possible air/polymer bubbles that were not able to get out, suggesting the sintering process is incomplete and that scattering loss may be present.

Figure 2 shows the refractive index profile of the sintered preform from the drop of the draw start, measured with a preform index analyzer (Photon Kinetics PK2600). Three layers are seen: the outer cladding (F300 quartz tube, ϕ = 2.80 mm), the 3D printed inner cladding ϕ = 1.81 mm) and the thermally cured core (ϕ ~ 0.17 mm). The index difference between outer and inner cladding is Δn ~ 2.3 × 10^{-4}. Some sporadic features attributed to air channels are

marked with purple stars. The effective index difference of the core is about $\Delta n_{eff} \sim 0.0066$, sufficiently low to allow single mode propagation for 125 μm fibre. This value is less than the predicted value ($\Delta n_{eff} \sim 0.0214$, assuming no loss of core material) from the starting composition, suggesting material loss and diffusion during the debinding and drawing processes. At this stage just as drawing begins, it is clear the preform has not fully fused.

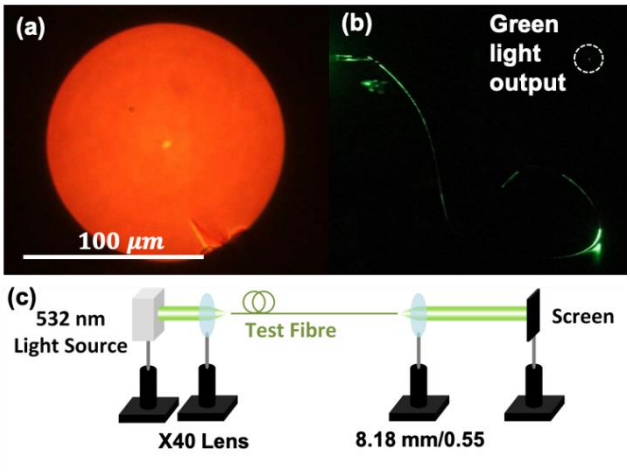

Fig. 3. (a) Fibre cross-section image of 3D printed single mode fibre; (b) transmission of $\lambda = 532$ nm through drawn fibre; and (c) photographic image of the transmission setup used. Strong scattering is observed.

Table 1. Loss of 3D printed single mode fibres at $\lambda = 532$ nm (diode pumped solid-state laser) and 632.8 nm (HeNe laser) and $\lambda = 1550$ nm (Er^{3+} fibre laser).

λ [nm]	532	633	1550
α [dB/m]	13.4	13.9	114

The fibre quality has been checked using an optical microscope. Fig. 3(a) and Fig 4 (a) shows the cross-section image of a typical 3D printed single mode (sm) fibre and multi-mode (mm). The fibre outer diameters are $\phi_{sm} = 131$ μm and $\phi_{sm} = 242$ μm respectively. The mm core is $\phi = 14$ μm and circular whilst the sm core is elliptical with minimum and maximum ellipse diameters $\phi_{sm\text{-}min} = 3.6$ μm and $\phi_{sm\text{-}max} = 4.8$ μm. This indicates a higher and more uniform tension is required during drawing. The experimental cutoff wavelength is $\lambda_c = 780$ nm, falling in between the estimated range from refractive index and core diameters. Launching green light ($\lambda = 532$ nm) through 2 m of fibre is shown in Fig. 3(c). The cutback loss at different wavelengths for the sm fibre is shown in Table 1. The near IR loss at 1550 nm arises from being above $\lambda_c = 780$ nm.

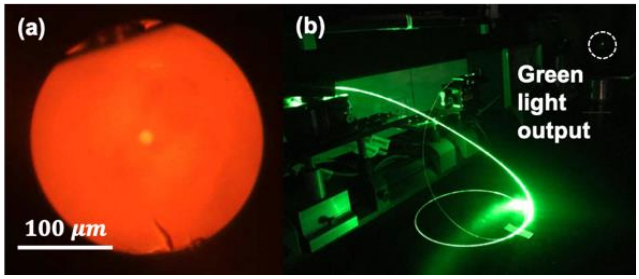

Fig. 4. (a) Fibre cross-section image of 3D printed multimode fibre; (b) transmission of $\lambda = 532$ nm light through drawn fibre; and (c) photographic image of the transmission setup used.

Losses in the green for the mm fibre, illustrated in Figure 4, are about twice as high arising from higher order mode coupling and leakage: $\alpha \sim 24$ dB/m @ $\lambda = 532$ nm, measured by cutback. On the other hand, propagation at 1550 nm is lower, ~ 5.5 dB/m, shown in the broadband measurements of Figure 5(b). This increased loss in the visible with the higher order modes indicates possible interfacial scattering from the observed air bubbles as the main source of loss. There also appears to be a significant contribution from water ($\lambda_{peak} = 1380$ nm where $\alpha = 20.9$ dB/m) suggesting the bubbles may contain trapped water consistent with incomplete sintering. This could be addressed by using both higher purity, drier starting chemicals and extending sintering and debinding. Removal of the outer silica tube, which can trap these impurities, may also improve these results, the subject of ongoing work.

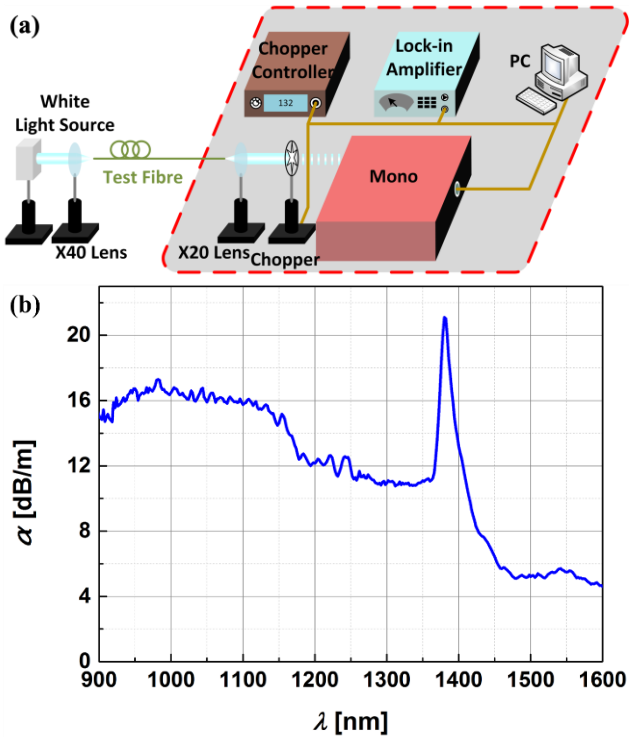

Fig. 5. (a) Experimental configuration of loss measurement by cutback technique; and (b) loss spectrum of the 3D printed multimode (mm) fibre.

In conclusion, whilst there remains considerable scope to improve the transmission properties of this fibre, the first single mode and multimode silica optical fibres have been drawn from a 3D printed preform. The relative ease in which this was achieved, suggests additive manufacturing will disrupt optical fibre fabrication. Unlike conventional labour intensive lathe-based methods, the design and fabrication is not limited by a centrally spun or finely stacked preform, enabling configurations such as improved multicore and complex optical fibres [6, 23-26], such as optimized Fresnel fibres, to be made. More broadly, painstakingly difficult complex patterns, multicore and multi-size and shaped fibres can be made that are otherwise not possible. This work, building off the original polymer versions, marks a new and exciting time for fibre fabrication and application.

Funding. Authors are thankful for the two LIEF grants (LE0883038 and LE100100098) by Australian Research Council (ARC) to fund the National Fibre Facility at UNSW, Sydney. The authors thank the Air Force Office of Scientific Research (AFOSR), in partnership of the Asian Office of Aerospace R&D (AOARD) and the High Energy Laser Joint Technology Office (HELJTO), for grant (FA2386-16-1-4031), and a National Science Foundation of China grant (61775045). Y. Chu and X. Fu also thank the support of the China Scholarship Council (CSC No. 201706680054 and 201708130199).

Disclosures. The authors declare no conflicts of interest.

References

1. G. D. Peng, Y. Luo, J. Zhang, J. Wen, Y. Chu, K. Cook, and J. Canning, in *Handbook of Optical Fibers*, Springer, ISBN 981-10-1477-2_79-1, 637 (2019).
2. J. Canning, and K. Cook, *in Conference on Lasers and Electro-Optics/Pacific Rim 2018* (Optical Society of American, 2018), p. F1B-1.
3. K. Cook, J. Canning, S. Leon-Saval, Z. Reid, M. A. Hossain, J. -E. Comatti, Y. Luo, and G. D. Peng, Opt. Lett. 40, 3966 (2015).
4. K. Cook, G. Balle, J. Canning, L. Chartier, T. Athanaze, M. A. Hossain, C. Han, J. -E. Comatti, Y. Luo, and G.D. Peng, Opt. Lett. 41, 4554 (2016).
5. Y. Luo, J. Wen, J. Zhang, J. Canning, and G. D. Peng, Opt. Lett. 37, 3447 (2012).
6. J. Canning, in Selected Topics in Photonic Crystals and Metamaterials, World Scientific, ISBN 978-981-4355-18-6C, 389 (2011).
7. J. Hao, Y. Chu, Z. Ma, Q. Chai, J. Ren, Y. Liu, Y. Luo, J. Yang, Z. Liu, J. Zhang, L. Yuan, and G. D. Peng, Opt. Fiber Technol. 46, 141 (2018).
8. A. Michie, J. Canning, I. Bassett, J. Haywood, K. Digweed, A. Lau, D. Scandurra, M. Aslund, B. Ashton, M. Stevenson and J. Digweed, Opt. Exp., 15 (4), 1811-1816, (2007)
9. Y. Chu, Y. Tian, D. Fan, G. Xiao, S. Wei, B. Zhang, X. Fu, Z. Ma, J. Ren, Q. Chai, Y. Luo, J. Zhang, and G. D. Peng, in CLEO: QELS_Fundamental Science 2019 (Optical Society of American, 2019), p. JW2A-107.
10. Y. Luo, Y. Chu, K. Cook, G. Tafti, S. Wang, W. Wang, Y. Tian, J. Canning, and G. D. Peng, in. Asia Communications and Photonics Conference 2018 (IEEE, 2018), p. 1-3.
11. J. Canning, M. A. Hossain, C. Han, L. Chartier, K. Cook, and T. Athanaze, Opt. Lett. 41, 5551 (2016).
12. W. Talataisong, R. Ismaeel, S. R. Sandoghchi, T. Rutirawut, G. Topley, M. Beresna and G. Brambilla, Opt. Exp., 26, 32007 (2018).
13. H. Bikas, P. Stavropoulos, and G. Chryssolouris, Int. J. Adv. Manuf. Technol. 83, 389 (2016).
14. Y. Yang, X. Song, X. Li, Z. Chen, C. Zhou, Q. Zhou, and Y. Chen, Adv. Mater. 30, 1706539 (2018).
15. A. Camposeo, L. Persano, M. Farsari, and D. Pisignano, Adv. Opt. Mater. 7, 1800419 (2019).
16. J. Klein, M. Stern, G. Franchin, M. Kayser, C. Inamura, S. Dave, J. C. Weaver, P. Houk, P. Colombo, M. Yang, and N. Oxman, 3D Print. Addit. Manuf. 2, 92 (2015).
17. F. Kotz, K. Arnold, W. Bauer, D. Schild, N. Keller, K. Sachsenheimer, T. M. Nargang, C. Richter, D. Helmer, and B. E. Rapp, Nature 544, 337 (2017).
18. F. Kotz, P. Risch, K. Arnold, S. Sevim, J. Puigmartí-Luis, A. Quick, M. Thiel, A. Hrynevich, P. D. Dalton, D. Helmer, D. and B. E. Rapp, Nat. Commun. 10, 1439 (2019).
19. D. T. Nguyen, C. Meyers, T. D. Yee, N. A. Dudukovic, J. F. Destino, C. Zhu, E. B. Duoss, T. F. Baumann, T. Suratwala, J. E. Smay, and R. Dylla-Spears, Adv. Mater. 29, 1701181 (2017).
20. J. F. Destino, N. A. Dudukovic, M. A. Johnson, D. T. Nguyen, T. D. Yee, G. C. Egan, A. M. Sawvel, W. A. Steele, T. F. Baumann, E. B. Duoss, T. Suratwala, and R. Dylla-Spears, Adv. Mater. Technol. 3, 1700323 (2018).
21. F. Kotz, K. Plewa, W. Bauer, N. Schneider, N. Keller, T. Nargang, D. Helmer, K. Sachsenheimer, M. Schäfer, M. Worgull, C. Greiner, C. Richter, B. E. Rapp, Adv. Mater. 28, 4646 (2016).
22. F. Kotz, N. Schneider, A. Striegel, A. Wolfschläger, N. Keller, M. Worgull, W. Bauer, D. Schild, M. Milich, C. Greiner, D. Helmer, B. E. Rapp, Adv. Mater. 30, 1707100 (2018).
23. A. Bjarklev, J. Broeng and A. S. Bjarklev, in Photonic Crystal Fibres, Springer, ISBN 978-1402076107, (2003).
24. W. Wang, G. Tafti, M. Ding, Y. Luo, Y. Tian, S. Wang, T. Karpisz, J. Canning, K. Cook and G. D. Peng, Frontiers in Optoelectronics 11, 69 (2018).
25. J. Canning, in Photonics Research Developments, Nova Science Publishers, ISBN 978-1-60456-720-5, Chap. 5 (2008).
26. C. Martelli and J. Canning, Opt. Exp. 15, 4281 (2007).

Full citation listings

1. G. D. Peng, Y. Luo, J. Zhang, J. Wen, Y. Chu, K. Cook and J. Canning, "3D Silica Lithography for Future Optical Fiber Fabrication." in *Handbook of Optical Fibers,* Springer, ISBN 981-10-1477-2_79-1, 637-653 (2019).
2. J. Canning, and K. Cook, "3D printing, photonics and the IoT," in *Conference on Lasers and Electro-Optics/Pacific Rim 2018* (Optical Society of American, 2018), p. F1B-1.
3. K. Cook, J. Canning, S. Leon-Saval, Z. Reid, M. A. Hossain, J. -E. Comatti, Y. Luo, and G. D. Peng, "Air-structured optical fiber drawn from a 3D-printed preform," Optics Letters **40**, 3966-3969 (2015).
4. K. Cook, G. Balle, J. Canning, L. Chartier, T. Athanaze, M. A. Hossain, C. Han, J. -E. Comatti, Y. Luo, and G.D. Peng, "Step-index optical fiber drawn from 3D printed preforms," Optics Letters **41**, 4554-4557 (2016).
5. Y. Luo, J. Wen, J. Zhang, J. Canning and G. D. Peng, "Bismuth and erbium codoped optical fiber with ultrabroadband luminescence across O-, E-, S-, C-, and L-bands," Optics Letters **37**, 3447-3449 (2012).
6. J. Canning, "Structured Optical Fibres and the Application of Their Linear and Non-Linear Properties," in *Selected Topics in Photonic Crystals and Metamaterials*, World Scientific, ISBN 978-981-4355-18-6C, 389-452 (2011).
7. J. Hao, Y. Chu, Z. Ma, Q. Chai, J. Ren, Y. Liu, Y. Luo, J. Yang, Z. Liu, J. Zhang, L. Yuan and G. D. Peng, "Effects of thermal treatment on photoluminescence properties of bismuth/erbium co-doped optical fibers," Optical Fiber Technology **46**, 141-146 (2018).
8. A. Michie, J. Canning, I. Bassett, J. Haywood, K. Digweed, A. Lau, D. Scandurra, M. Aslund, B. Ashton, M. Stevenson and J. Digweed, "Spun elliptically birefringent photonic crystal fibre," Optics Express **15**, 1811-1816 (2007).
9. Y. Chu, Y. Tian, D. Fan, G. Xiao, S. Wei, B. Zhang, X. Fu, Z. Ma, J. Ren, Q. Chai, Y. Luo, J. Zhang and G. D. Peng, "Fabrication and Characterization of Birefringent Bismuth and Erbium Co-Doped Photonic Crystal Fiber for Broadband Polarized Near Infrared Emission," in *CLEO: QELS_Fundamental Science 2019* (Optical Society of American, 2019), p. JW2A-107.
10. Y. Luo, Y. Chu, K. Cook, G. Tafti, S. Wang, W. Wang, Y. Tian, J. Canning and G. D. Peng "Spun High Birefringence Bismuth/Erbium Co-Doped Photonic Crystal Fibre with Broadband Polarized Emission," in. *Asia Communications and Photonics Conference 2018* (IEEE, 2018), p. 1-3.
11. J. Canning, M. A. Hossain, C. Han, L. Chartier, K. Cook, and T. Athanaze, "Drawing optical fibers from three-dimensional printers," Optics Letters **41**, 5551-5554 (2016).
12. W. Talataisong, R. Ismaeel, S. R. Sandoghchi, T. Rutirawut, G. Topley, M. Beresna and G. Brambilla, "Novel method for manufacturing optical fiber: extrusion and drawing of microstructured polymer optical fibers from a 3D printer," Opt. Exp., **26**, 32007-32013 (2018).
13. H. Bikas, P. Stavropoulos and G. Chryssolouris, "Additive manufacturing methods and modelling approaches: a critical review," The International Journal of Advanced Manufacturing Technology **83**, 389-405 (2016).
14. Y. Yang, X. Song, X. Li, Z. Chen, C. Zhou, Q. Zhou, and Y. Chen, "Recent Progress in Biomimetic Additive Manufacturing Technology: From Materials to Functional Structures," Advanced Materials **30**, 1706539 (2018).
15. A. Camposeo, L. Persano, M. Farsari, and D. Pisignano, "Additive Manufacturing: Applications and Directions in Photonics and Optoelectronics," Advanced Optical Materials **7**, 1800419 (2019).
16. J. Klein, M. Stern, G. Franchin, M. Kayser, C. Inamura, S. Dave, J. C. Weaver, P. Houk, P. Colombo, M. Yang, and N. Oxman, "Additive manufacturing of optically transparent glass," 3D Printing Additive Manufacturing. **2**, 92-105 (2015).
17. F. Kotz, K. Arnold, W. Bauer, D. Schild, N. Keller, K. Sachsenheimer, T. M. Nargang, C. Richter, D. Helmer, and B. E. Rapp, "Three-dimensional printing of transparent fused silica glass" Nature **544**, 337-339 (2017).
18. F. Kotz, P. Risch, K. Arnold, S. Sevim, J. Puigmartí-Luis, A. Quick, M. Thiel, A. Hrynevich, P. D. Dalton, D. Helmer, D. and B. E. Rapp, "Fabrication of arbitrary three-dimensional suspended hollow microstructures in transparent fused silica glass," Nature Communications **10**, 1439 (2019).
19. D. T. Nguyen, C. Meyers, T. D. Yee, N. A. Dudukovic, J. F. Destino, C. Zhu, E. B. Duoss, T. F. Baumann, T. Suratwala, J. E. Smay, and R. Dylla-Spears, " 3D ‐ printed transparent glass," Advanced Materials **29**, 1701181 (2017).
20. J. F. Destino, N. A. Dudukovic, M. A. Johnson, D. T. Nguyen, T. D. Yee, G. C. Egan, A. M. Sawvel, W. A. Steele, T. F. Baumann, E. B. Duoss, T. Suratwala, and R. Dylla-Spears, "3D printed optical quality silica and silica–titania glasses from sol–gel feedstocks," Advanced Materials Technologies **3**, 1700323 (2018).
21. F. Kotz, K. Plewa, W. Bauer, N. Schneider, N. Keller, T. Nargang, D. Helmer, K. Sachsenheimer, M. Schäfer, M. Worgull, C. Greiner, C. Richter, B. E. Rapp, "Liquid glass: a facile soft replication method for structuring glass," Advanced Materials **28**, 4646-4650 (2016).
22. F. Kotz, N. Schneider, A. Striegel, A. Wolfschläger, N. Keller, M. Worgull, W. Bauer, D. Schild, M. Milich, C. Greiner, D. Helmer, B. E. Rapp, "Glassomer—processing fused silica glass like a polymer," Advanced Materials **30**, 1707100 (2018).
23. A. Bjarklev, J. Broeng and A. S. Bjarklev, in *Photonic Crystal Fibres*, Springer, ISBN 978-1402076107, (2003).
24. W. Wang, G. Tafti, M. Ding, Y. Luo, Y. Tian, S. Wang, T. Karpisz, J. Canning, K. Cook and G. D. Peng, "Structure formation dynamics in drawing silica photonic crystal fibres," Frontiers in Optoelectronics **11**, 69-76 (2018).
25. J. Canning, in *Photonics Research Developments*, Nova Science Publishers, ISBN 978-1-60456-720-5, Chapter 5 (2008).
26. C. Martelli and J. Canning, "Fresnel fibres with omnidirectional zone cross-sections" Optics Express **15**, 4281-4286 (2007).